JIPB Journal of Integrative Plant Biology

Maize *WI5* encodes an endo-1,4-β-xylanase required for secondary cell wall synthesis and water transport in xylem[OO]

Xiaojiao Hu†, Yang Cui†, Xiaomin Lu, Weibin Song, Lei Lei, Jinjie Zhu, Jinsheng Lai, Lizhu E* and Haiming Zhao*

State Key Laboratory of Plant Physiology and Biochemistry, National Maize Improvement Center, College of Agronomy and Biotechnology, China Agricultural University, Beijing 100193, China
†These authors contributed equally to this work
*Correspondences: Haiming Zhao (haiming223@163.com, Dr. Zhao is responsible for the distribution of the materials associated with this article); Lizhu E (elizhu@cau.edu.cn)
doi: 10.1111/jipb.12923

Research Article

Abstract Water transport from roots to leaves through xylem is important for plant growth and development. Defects in water transport can cause drought stress, even when there is adequate water in the soil. Here, we identified the maize (*Zea mays*) *wilty5* (*wi5*) mutant, which exhibits marked dwarfing and leaf wilting throughout most of its life cycle under normal growth conditions. *wilty5* seedlings exhibited lower xylem conductivity and wilted more rapidly under drought, NaCl, and high temperature treatments than wild-type plants. Map-based cloning revealed that *WI5* encodes an active endo-1,4-β-xylanase from glycosyl dehydration family 10, which mainly functions in degrading and reorganizing cell wall xylan. Reverse-transcription polymerase chain reaction and β-glucuronidase assays revealed that *WI5* is highly expressed in stems, especially in internodes undergoing secondary wall assembly. RNA sequencing suggested that *WI5* plays a unique role in internode growth. Immunohistochemistry and electron microscopy confirmed that *wi5* is defective in xylan deposition and secondary cell wall thickening. Lignin deposition and xylan content were markedly reduced in *wi5* compared to the wild-type plants. Our results suggest that *WI5* functions in xylem cell wall thickening through its xylanase activity and thereby regulates xylem water transport, the drought stress response, and plant growth in maize.

Edited by: Zhizhong Gong, China Agricultural University, China
Received Jun. 16, 2019; **Accepted** Feb. 23, 2020; **Online on** Mar. 4, 2020
OO: OnlineOpen

OnlineOpen

INTRODUCTION

The cell wall functions not only as a physical barrier and the first line of defense between the plant cell and the external environment, but it is also a flexible, responsive structure involved in regulating plant growth (Seifert and Blaukopf 2010; Wolf et al. 2012). The plant cell wall is a composite structure consisting of cellulose microfibrils embedded in a matrix of hemicelluloses, pectins, and proteins. The cell walls of typical grass plants contain approximately 55% hemicellulose, 25% cellulose, and only 10% pectin. Glucuronoarabinoxylan is the major component of hemicellulose, comprising 20%–40% of the primary cell wall and 40%–50% of the secondary cell wall (Lerouxel et al. 2006; Vogel 2008). Plant cell walls have the remarkable property of extreme tensile strength combined with extensibility. Genes associated with cell wall thickening often contribute to the mechanical properties of the cell wall in structures such as the xylem of vascular bundles and in epidermal cells. *Arabidopsis thaliana* KNAT7 regulates secondary cell wall biosynthesis and thickening through directly activating the promoters of xylan

biosynthetic genes, an essential process in the development of xylem cells with normal morphology (Liu et al. 2014; He et al. 2018). Mutants in some kinds of endo-beta-1,4-glucanases resulted in changes in crystallinity of cellulose, which affect secondary cell wall development (Glass et al. 2015).

The upward growth and transpiration of terrestrial plants present challenges to water transport capacity. Water is transported from roots to leaves through xylem, and xylem impairment impedes water transport (Yuan et al. 2007; Venturas et al. 2017). The water transport capacity of xylem is determined by the unique structure of its cell wall, especially the secondary cell wall. Increased cellulose synthesis and cell wall elasticity contribute to the maintenance of cell turgor and ensure normal water transport in plants. Several *Arabidopsis* mutants with interrupted cell wall synthesis show increased sensitivity to abiotic stress. The *lew3* mutant, with impaired cellulose synthesis and collapsed xylem, is more sensitive to salt stress and loses less water through transpiration than the wild-type (Zhang et al. 2009a). The *sos6* mutant, containing a mutation in a cellulose synthase-like protein gene, is hypersensitive to salt and oxidative stress (Zhu et al. 2010). Cellulose synthase CESA6 and cellulose synthase-interactive protein CSI1 are involved in cellulose deposition and essential for salt stress (Zhang et al. 2016). By contrast, disrupting the cellulose synthesis gene, *AtCesA8,* results in enhanced drought and osmotic stress tolerance in *Arabidopsis* (Chen et al. 2005). Several cellulose synthesis -associated genes that affect water transport have been reported in rice (*Oryza sativa*). MicroRNA166 (miRNA166) regulates cellulose synthesis genes by targeting *OsBH4*. Knockdown of miRNA166 resulted in plants with xylem vessels with reduced diameters and stems with reduced water conductivity (Zhang et al. 2018). Rice *CLD1/SRL1* encodes a glycophosphatidylinositol (GPI)-anchored membrane protein; the loss-of-function of *CLD1/SRL1* leads to significant decreases in cellulose and lignin contents in the secondary cell walls of leaves, resulting in rapid water loss and leaf rolling (Li et al. 2017).

Several types of cell wall-related proteins function in cell wall remodeling, including glycoside hydrolases (GHs), glycosyltransferases, expansins, and peroxidase. GHs are broadly distributed enzymes that hydrolyze glycosidic bonds, leading to inversion and retention of the anomeric configuration of molecules (Ma et al. 2015; Wan et al. 2015). Plant GHs belong to 29 families, most of which were identified in *Arabidopsis* and rice. Endo-β-1,4-xylanases are major members of the plant GH family 10 (GH10). These enzymes play important roles in hydrolyzing xylan backbones into shorter, soluble xylo-oligo saccharides (Pollet et al. 2010). Two xylanases are strongly expressed during germination in barley (*Hordeum vulgare*), which primarily function in mobilizing nutrients from the aleurone layer and endosperm to the developing seed (Caspers et al. 2001). Maize (*Zea mays*) xylanase (Xyl) is thought to be involved in hydrolyzing the tapetum cell wall or stigma cell wall to facilitate pollen tube penetration into the silk (Li et al. 2012; Andriotis et al. 2016). *AtXyn1*, which is mainly expressed in *Arabidopsis* vascular bundles, is involved in rearranging or altering the orientation of hemicelluloses in the secondary cell wall (Suzuki et al. 2002). Members of GH10 are usually associated with carbohydrate binding domains (CMBs). Carbohydrate binding domains are structurally diverse noncatalytic domains that typically target enzymes to specific polysaccharide substrates and potentiate the activity of these enzymes against insoluble substrates such as cellulose, mannan, and xylan. Carbohydrate binding domains have been classified into 64 families (Cantarel et al. 2009), most of which have not been functionally characterized. Family 4 members display specificity for different polysaccharides, including amorphous cellulose, α-1,3-glucan, and xylan (Kognole and Payne 2015).

In maize, several wilty mutants—including the recessive mutant *wilty1* and dominant mutants *wilty2*, *wilty3* and *wilty2445*—have been previously described (Rock and Ng 1999). All of these mutants appear to be defective in vascular element development. None exhibited defects in the metabolism or signaling of abscisic acid (ABA), an important hormone for plant stomatal movement and drought tolerance. However, no wilty gene has been cloned to date, and the molecular mechanism underlying leaf wilting in maize is unknown. In the current study, we isolated and characterized the maize *wilty5* (*wi5*) mutant, which exhibits marked dwarfing and chronic leaf wilting, even under normal growth conditions. *WILTY5* encodes an active endo-1, 4-β-xylanase from the GH10 family. Our findings suggest that *WI5* functions in the formation of the secondary cell wall and plays an essential role in increasing the thickness of the internode xylem required for efficient water transport, thereby helping plants develop normally under high transpiration and water-stress conditions.

RESULTS

Identification of the drought-sensitive mutant *wi5* in maize

A wilty mutant, designated as *wi5* (*wilted5*), was isolated from a maize *Mutator* (*Mu*) mutagenized M_2 population. Under normal field conditions, *wi5* plants displayed a drought-sensitive phenotype, with wilting and progressive leaf chlorosis after the 3-leaf stage; these symptoms were the most pronounced in young leaves (Figure 1A). This mutant phenotype was more severe and developed earlier under drought or high-temperature conditions. The *wi5* mutant also exhibited marked dwarfing and reduced biomass (Figure 1B). Wilting occurred primarily at the leaf tips and spread around the leaf margins. Chlorosis developed after the leaves had fully expanded, followed by necrosis, which increased in severity during growth (Figure 1C). However, germination was unaffected in the mutant seeds, and no abnormal seedling phenotypes were observed.

We crossed *wi5* plants with B73 plants. All F_1 plants displayed a wild-type phenotype. Progeny derived from backcrossing F_1 to *wi5* plants showed an approximately 1:1 segregation ratio of wild-type : *wi5* mutant phenotypes, suggesting that *wi5* is a single-gene recessive nuclear mutant (Table S1).

Phenotypic and physiological characterization of *wi5* plants

When plants encounter drought stress, an array of physiological and biochemical modifications become activated, including leaf wilting, reduced stomatal conductance, impaired photosynthesis and reduced growth rates. The chlorotic appearance of *wi5* leaves suggests that this mutant has defects in photosynthetic pigment accumulation and photosynthesis. We therefore quantified photosynthetic pigment levels, photosynthesis rates, and other related physical indexes in wild-type and *wi5* plants. We detected

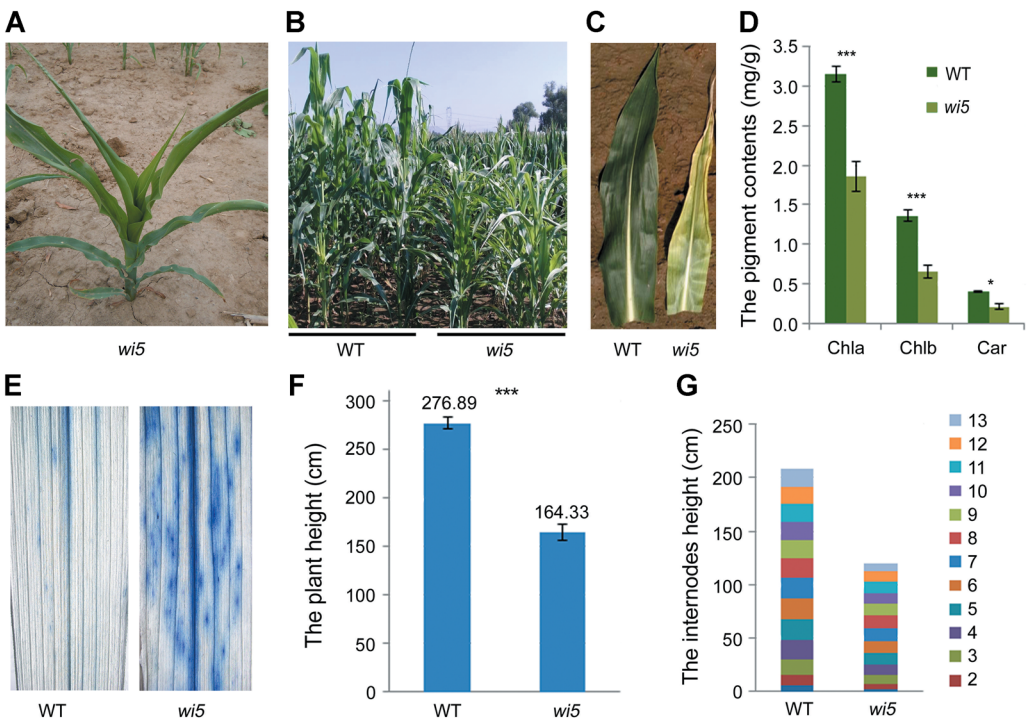

Figure 1. Phenotype of *wilty5* (*wi5*) plants under normal growth conditions

(**A**) Phenotype of *wi5* plants at the 8-leaf stage. (**B**) Phenotype of *wi5* plants at the tasseling stge. WT, wild-type. (**C**) Leaves of *wi5* and wild-type plants. (**D**) Pigment contents of *wi5* and wild-type leaves. Average of nine plants for *wi5* and wild-type respectively. Error bars indicate ± *SE*. $P_{Chla} = 0.000192866$, $P_{Chlb} = 0.000424478$, $P_{Car} = 0.041379928$, Student's *t*-test (**P* < 0.05, ***P* < 0.01, ****P* < 0.001). (**E**) Trypan blue staining of the leaves of wild-type and *wi5* plants. (**F**) Comparison of plant height between *wi5* and wild-type plants, *n* = 5 repeats, 10 plants per repeat. Error bars indicate ± *SE*. P = 5.30418E-13, Student's *t*-test (**P* < 0.05, ***P* < 0.01, ****P* < 0.001). (**G**) Comparison of overground internodes length between *wi5* and wild-type plants.

an approximately 40% and 20% reduction in chlorophyll (Chl) and carotenoid (Car) levels in *wi5* leaves compared to those of the wild-type, respectively (Figure 1D). The photosynthetic indicators of *wi5* plants were also strongly reduced relative to the wild-type (Table S2). The net photosynthetic rate (Pn) of *wi5* was strongly suppressed, and stomatal conductance (Cond), intercellular CO_2 concentration (Ci), and transpiration rate (Tromml) were sharply reduced (by approximately 66%–90%) compared to the wild-type.

We stained leaves of *wi5* and wild-type plants with Trypan blue, a histochemical indicator of irreversible membrane damage or cell death. Deep blue staining was observed in *wi5* leaves, whereas no obvious staining was detected in wild-type leaves (Figure 1E). These results suggest that *wi5* plants exhibit severe cellular damage and an impaired photosynthetic system. Furthermore, *wi5* plants displayed stunted growth, with a height approximately 60% that of wild-type plants at the mature stage (Figure 1F). Finally, we compared the elongation patterns of internodes in *wi5* and wild-type plants. Mutant and wild-type plants had the same number of internodes, but all *wi5* internodes were shorter than those of the wild-type (Figure 1G). The wilting and chlorotic leaves, impaired photosynthetic system, and stunted growth of *wi5* suggest that these plants suffer water stress, even under normal growth conditions.

wilted5 plants are hypersensitive to drought, high temperature, and NaCl at the seedling stage

At the seedling stage, *wi5* plants were indistinguishable from wild-type plants under greenhouse conditions. However, *wi5* plants were more sensitive than wild-type plants to drought, high temperature (42°C), or NaCl stress, exhibiting severely suppressed growth and significantly reduced survival rates under these conditions. Figure 2A shows wild-type and *wi5* plants grown for 3 weeks in the same pot and treated with drought stress by withholding water. After 10 d of drought treatment, wild-type leaves remained turgid, whereas *wi5* leaves showed obvious wilting. After an additional 10 d, the wilting of *wi5* was more severe than that of the wild-type. When water was withheld from the soil for 30 d, both wild-type and *wi5* plants wilted. After watering was resumed, 80% of wild-type plants survived, whereas all *wi5* plants died.

The *wi5* plants were also more sensitive than wild-type plants to high-temperature stress (Figure 2B). When treated with 42°C for 12 h, *wi5* plants showed earlier leaf rolling and wilting than the wild type. After 48 h of treatment, the blades of *wi5* leaves curled sharply downward, whereas those of wild-type plants remained erect.

Since crosstalk occurs between drought and salt tolerance (Liu et al. 2010; Chien Van et al. 2014; Guo et al. 2016), we also examined the responses of *wi5* and wild-type plants to a 250 mmol/L NaCl treatment (Figure 2C). Similar to the results of drought treatment, after 6 d of watering with 250 mmol/L NaCl, the growth of *wi5* plants was completely suppressed, and the plants were more wilted and chlorotic than wild-type plants.

wilted5 mutants exhibit a hypersensitive response to water stress, but impaired water transport system

To determine why *wi5* plants are hypersensitive to drought stress and have an impaired water transport capacity, we analyzed the ABA contents, reactive oxygen species accumulation, water loss rate of isolated leaves, and injury flow of the seedlings. Drought treatment induced an increase in ABA content—both *wi5* and wild-type plants accumulated up to four times more ABA under drought conditions than well-watered conditions—and there was no significant difference in ABA contents between the mutant and wild-type leaves (Figure 3A).

H_2O_2 accumulation was monitored by 3,3′-diaminobenzidine (DAB) staining. Before osmotic stress treatment, little staining was observed in *wi5* and wild-type plants (left side of Figure 3B). After 24 h of treatment with 20% polyethylene glycol (PEG) and 30 μmol/L methyl viologen (MV), H_2O_2 accumulation was observed in both the mutant and wild-type (right side of Figure 3B). In the detached leaves of 3-week-old seedlings, water loss was a little slower for *wi5* than the wild-type (Figure 3C); the *wi5* mutant also displayed lower stomatal conductance than the wild-type (Table S2). These results imply that *wi5* plants can prevent water loss by closing their stomata and therefore have a normal physiological response to drought stress.

Furthermore, *wi5* seedlings had a significantly lower injury flow rate than the wild-type (Figure 3D),

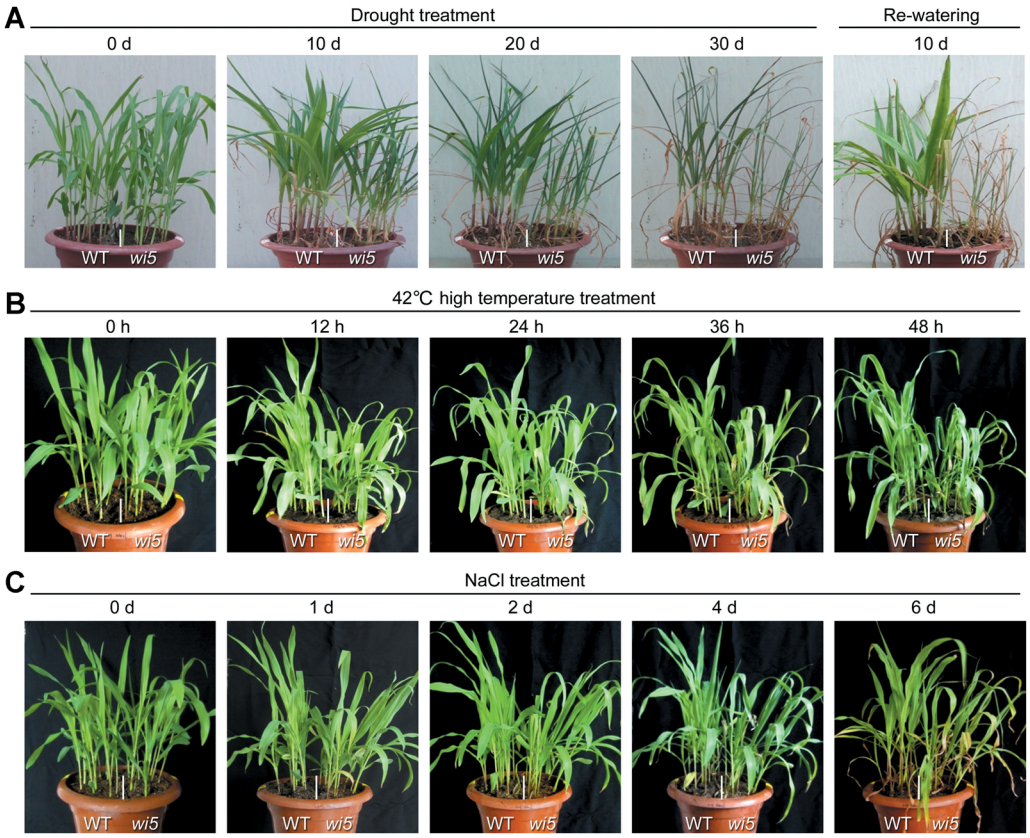

Figure 2. Abiotic stress response of *wilty5* (*wi5*) plants at the seedling stage
Wild-type and *wi5* plants at the 3-leaf stage were grown in the same pots filled with a mixture of soil and vermiculite (2:1). The left and right half of each pot was planted with 10 wild-type and 10 *wi5* mutant plants, respectively. (**A**) Plants were not watered for 0, 10, 20, or 30 d, followed by re-watering for 10 d. (**B**) Plants were treated at 42°C for 0, 12, 24, 36, and 48 h. (**C**) Plants were watered with 250 mmol/L NaCl for 0, 1, 2, 4, and 6 d. Photographs were taken after each treatment.

indicating that the wilty phenotype of *wi5* is the result of an impaired water transport system.

Map-based cloning and complementation of the *wi5* mutant

We performed map-based cloning to isolate the *WI5* gene using a BC_1F_1 segregating population generated from a cross between the *wi5* mutant and wild-type cultivar B73. The *WI5* locus was initially mapped to the short arm of chromosome 5 in a 19-cM region between the two simple sequence repeat (SSR) markers bnlg1660 and umc2167 (Figure 4A). To determine the precise position of *WI5*, we used a larger BC_1F_1 mapping population consisting of 3,800 plants for fine mapping. One InDel marker (IDP), two SSR markers, and two cleaved-amplified polymorphic sequence (CAPS) markers were developed (Table S3) between markers umc2115 and umc2293. The *WI5* locus was mapped to a 50-kb DNA region between markers 082IDP and Caps2 on a single bacterial artificial chromosome (BAC), AC208082. Within this region, three open reading frames (ORFs) were predicted using the program FGENESH (www.softberry.com), but only one expressed gene was identified. Reverse-transcription polymerase chain reaction (RT-PCR) analysis revealed that the candidate gene is 2,247 bp long, with three exons and two introns and encoding a 748 amino acid protein known as endo-1,4-β-xylanase. The *wi5* allele contains a 20-bp deletion in the first exon that results in a frame-shift mutation, an early stop codon, and a truncated protein with 178 amino acids (Figure 4B). Thus, the mutation might severely reduce or completely disrupt the activity of the protein. A Basic Local Alignment Search Tool search revealed only one copy of *WI5* in the maize genome.

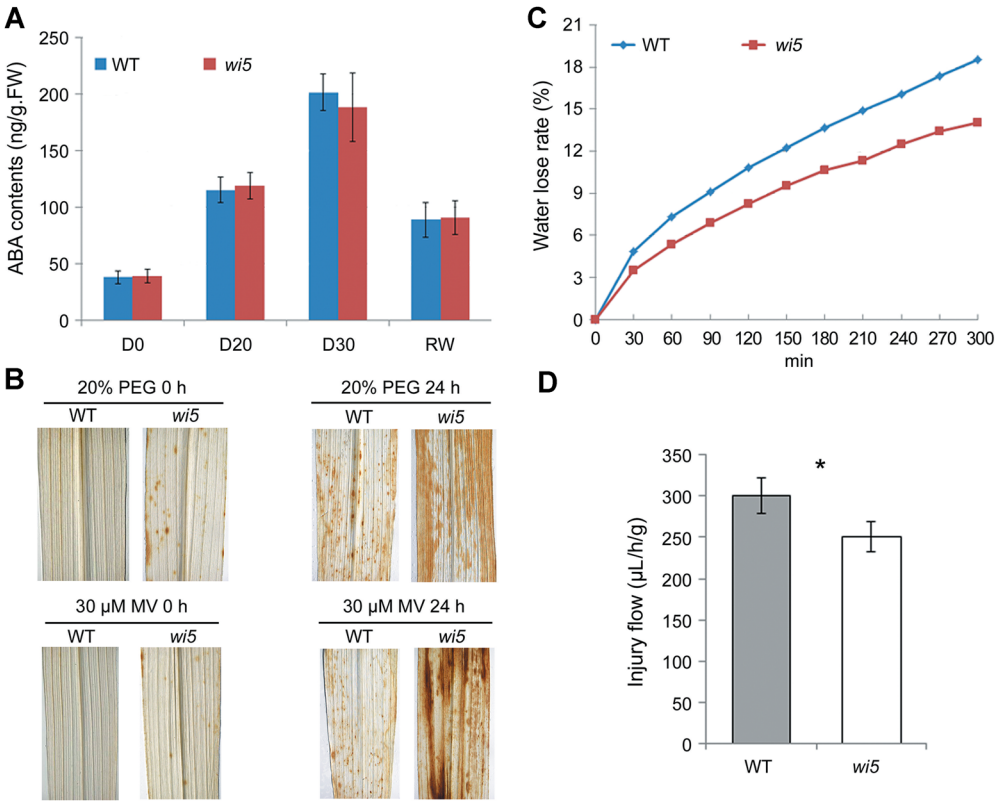

Figure 3. Analysis of abscisic acid (ABA) contents, reactive oxygen species (ROS) accumulation, water loss rate of detached leaves, and injury flow of seedlings

(**A**) ABA contents of wild-type and *wilty5* (*wi5*) plants under different water conditions. D0, 3-week-old seedlings watered normally; D20, 20 d drought treatment; D30, 30 d drought treatment; RW, re-watering. Error bars indicate ± *SE* ($n = 3$). $P_{D0} = 0.91053919$, $P_{D20} = 0.714923541$, $P_{D30} = 0.540158035$, $P_{RW} = 0.897058614$, Student's *t*-test (**P* < 0.05, ***P* < 0.01, ****P* < 0.001). (**B**) 3,3′-diaminobenzidine (DAB) staining for H_2O_2 in wild-type and *wi5* leaves from plants at the 3-leaf stage. *wi5* and wild-type plants at the 3-leaf stage were treated with 20% (w/v) polyethylene glycol (PEG) and 30 μm methyl viologen (MV) solution for 24 h. (**C**) Water loss of wild-type and *wi5* plants. For each repeat, fully expanded leaves of 14-d-old plants were analyzed in a triplicate experiment. (**D**) Comparison of injury flow in wild-type and *wi5* 3-leaf seedlings. Error bars indicate ± *SE* ($n = 3$). $P = 0.034$, Student's *t*-test (**P* < 0.05, ***P* < 0.01, ****P* < 0.001).

We carried out a complementation test to confirm the mapping results. As *wi5* is not a suitable transgene acceptor, we transferred a 4.632-kb wild-type DNA fragment containing the *WI5* promoter region and the entire ORF into a wild-type acceptor in the X178 background. We crossed positive T0 plants with *wi5* plants and determined that half of the F_1 progeny harbored the transferred DNA. The positive F_1 plants were self-pollinated to obtain an F_2 population. Approximately 1/16 of the F_2 plants exhibited the wilting and stunted growth phenotypes characteristic of *wi5* (Table S4). We isolated an unsegregated F_3 line and determined (by droplet digital PCR (ddPCR)) that it was a single copy event (Figure S1). These results demonstrate that *WI5* is indeed responsible for the phenotypic changes observed in the *wi5* mutant.

Tissue-specific expression profiles of *WI5*

To obtain further insight into the *wi5* phenotype, we investigated the tissue-specific expression patterns of *WI5* by quantitative RT-PCR. Although *WI5* was expressed in all of the organs examined, it was expressed at the highest level in the developing stem and at very low levels in the ear, seed, embryo, and endosperm (Figure 5A). We then examined the transcript profiles of *WI5* in various internodes in the stems of maize plants at the flowering stage. *WI5* messenger RNA levels varied along the length of the stem, with higher expression in the middle internodes

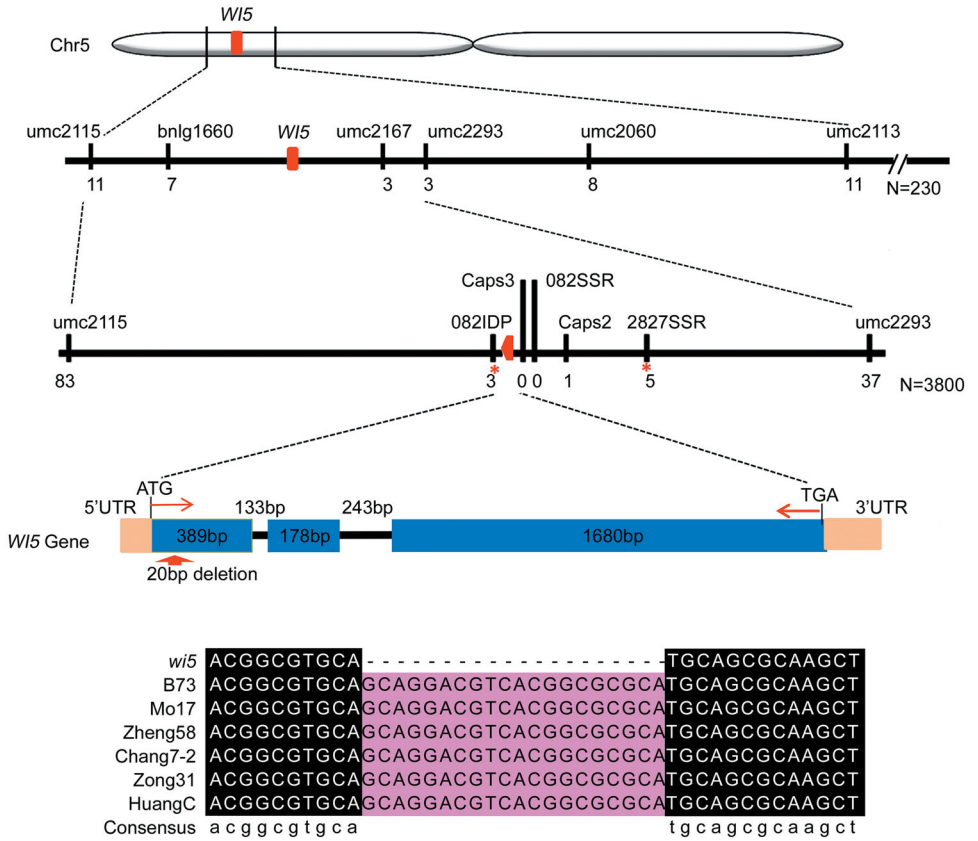

Figure 4. Map-based cloning of *WILTY5 (WI5)*

(**A**) The *WI5* locus was mapped onto chromosome 5 between markers bnlg1660 and umc2167 using 230 BC_1F_1 plants. After fine mapping, the *WI5* locus was narrowed to a 50 kb region between markers 082IDP and Caps2 using 3800 BC_1F_1 plants. Numbers below the horizontal line are the number of recombinants. (**B**) The gene structure of *wi5*. A 20-bp deletion (pink shading) in the first exon of *wi5* leads to a frame-shift mutation and an early stop codon. Nucleic acid sequence alignment of *WI5* from *wi5* and six inbred lines.

(eighth and ninth internodes, counted from the base of the plant) and lower expression in the basal and upper internodes (Figure 5B). The middle internodes were nonelongating internodes that had recently stopped elongating and were undergoing secondary cell wall assembly. These results suggest that *WI5* contributes to secondary cell wall modification in maize.

To investigate the expression pattern of *WI5* in more detail, we produced transgenic plants carrying the β-glucuronidase (GUS) reporter gene driven by the 1.5-kb promoter region upstream of *WI5*. GUS activity was predominantly localized to the vascular and epidermal tissues of the stem, a site of secondary cell wall deposition (Figure 5F, G). Some activity was also evident in the vascular tissue of the leaf sheaths (Figure 5D, E), but it was completely absent in younger leaves and roots (Figure 5C, H).

Since the *wi5* mutant exhibited wilting leaves and short internodes, we were interested in determining whether the transcript levels of genes were altered in these tissues. We analyzed RNA-seq data for the 13th leaves and eighth internodes of wild-type and *wi5* plants. Principal component analysis (PCA) revealed that the transcripts in internodes were significantly different between the wild-type and mutant, while those in leaves were only slightly different (Figure S2A). More differentially expressed genes (DEGs) were identified in the internodes than in the leaves based on PCA (Figure S2B). Kyoto Encyclopedia of Genes and Genomes (KEGG) pathway enrichment analysis of internode data revealed many genes involved in synthesis and metabolism pathways that were down-regulated in *wi5* internodes, in alignment with the repressed cell growth. Furthermore, genes that

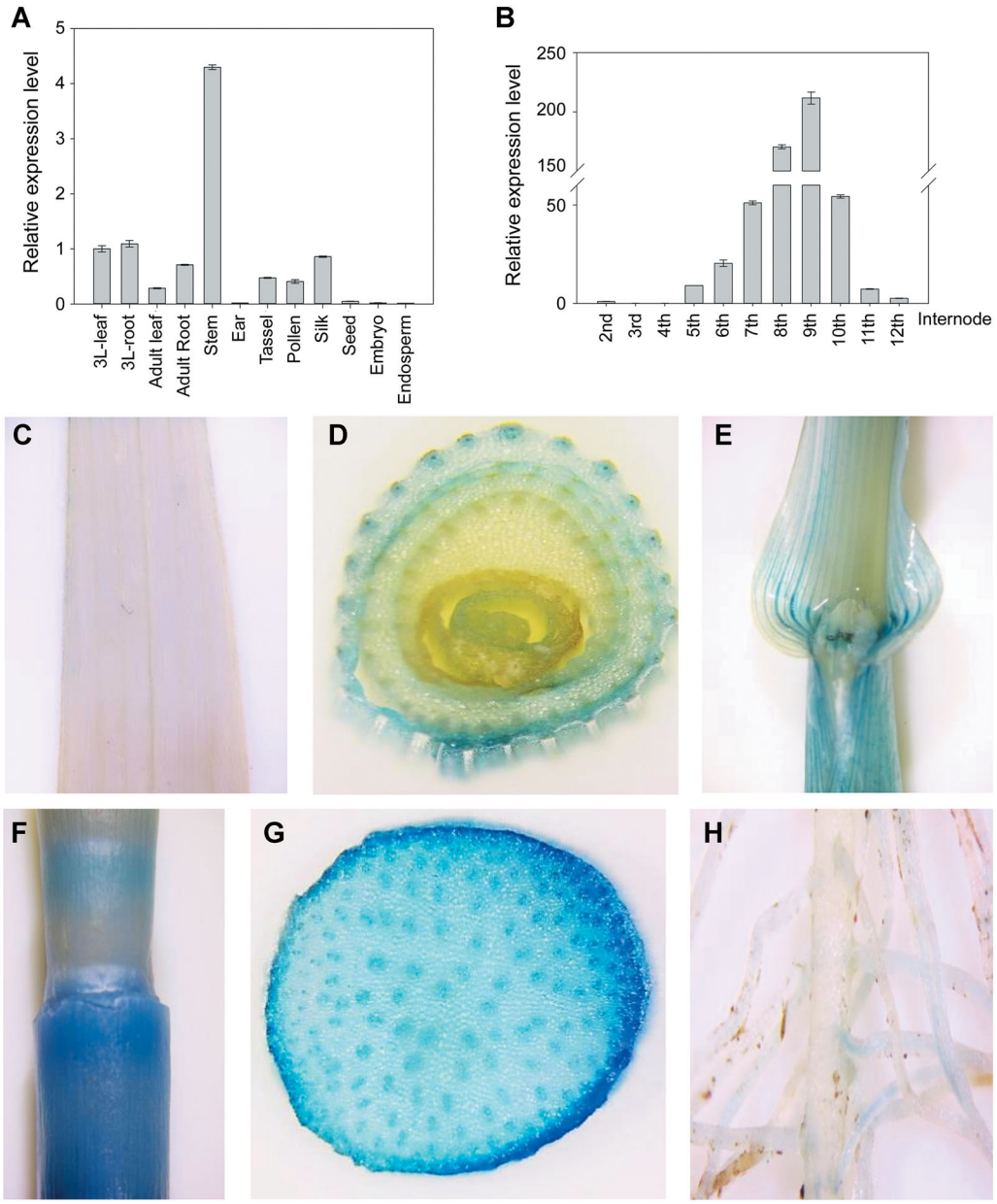

Figure 5. Expression profile of *WILTY5 (WI5)*

(A) Expression levels of *WI5* in various tissues. Twelve tissues or organs were examined as follows: leaves from seedlings at the 3-leaf stage (3L-leaf); roots from seedlings at the 3-leaf stage (3L-root); adult leaves; adult roots; stems; ears; tassels; pollen; silk; seeds; embryos; endosperms. (**B**) Expression levels of *WI5* in different internodes. (**C**–**H**) Transgenic plants carrying the β-glucuronidase (GUS) reporter gene driven by the *WI5* promoter. (**C**) Young leaf; (**D**) cross-section of a leaf sheath; (**E**) leaf sheath; (**F**) internode; (**G**) cross-section of an internode; (**H**) root.

function in DNA replication and repair were up-regulated in these mutant internodes, likely to compensate for their metabolic deficiency (Figure S2C). These results suggest that *WI5* is primarily expressed in internodes, functions in metabolic pathways, and mediates water transport and normal growth in the middle internodes.

WILTED5 encodes a GH10 family member

The GH10 family consists of endo-1,4-β-xylanases (EC3.2.1.8), endo-1,3-β-xylanases (EC 3.2.1.32), and cellobiohydrolases (EC 3.2.1.91). The major enzymes of this family are endo-1,4-β-xylanases, which are widely distributed among phyla, including numerous bacteria, fungi, and plant species. Endo-1,4-β-xylanases comprise

both catalytic and noncatalytic modules held together by flexible linker regions. The PFAM (protein families database of alignments and hidden Markov models) prediction program indicated that WI5 contains two carbohydrate binding domains (CBM-4-9 and pfam02018) arranged in tandem at its N-terminus and one GH10 catalytic domain (pfam00331) at its C-terminus (Figure 6A).

Analysis of the complete genome sequence of maize revealed ten GH10 family members of *WI5*, which were designated as *Zmxyl1* to *Zmxyl10*. Bioinformatics analysis revealed that these genes are located on different maize chromosomes, sharing 20% –50% identity with *WI5* (Table S5). To determine the evolutionary relationships of maize GH10 family genes and xylanase genes of other species, we built a rooted phylogenetic tree using the neighbor-joining method (Figure 6B). Phylogenetic analysis revealed that these genes are divided into two subfamilies. Genes from different clades might have different functions. *WILTED5* and *Zmxyl1*, *2*, *3*, and *4* belong to one clade and *WI5* and *Atxyn1* from *Arabidopsis* form a monophyletic clade with 88% bootstrap support. As *Atxyn1* functions in secondary cell wall metabolism in vascular bundle cells (Suzuki et al. 2002), we propose that *WI5* might have a similar function in maize.

The overall structure of the catalytic domain of GH10 xylanases is a cylindrical eightfold α/β barrel resembling a salad bowl, with two active-site glutamates, one of which is the nucleophile and the other the acid-base (Juturu and Wu 2012). Site-directed mutagenesis studies identified Glu-128 and Glu-236 as essential residues in the active site of xylanase A from *Streptomyces lividans*. Asp-124 also contributes to the catalytic mechanism (Ding and Cai 2013). The active site of GH10 proteins predicted in PROSITE is [GTA]-X-X-[LIVN]-x-[IVMF]-[ST]-E-[LIY]-[DN]-[LIVMF].

We compared the reported xylanase catalytic domains of different organisms (Figure 6C), including various plant species such as *Hordeum vulgare* (barley X-I, X-II), *Arabidopsis thaliana* (Atxy1), *Zea mays* (xyl), *Streptomyces lividans* (Xylanase A), and *Penicillium simplicissimum* (xynA). WILTED5 and the other xylanases share a high level of sequence similarity over regions surrounding the enzymatic active site within the GH10 domain. Two nucleophilic residues (glutamic acid and asparagine) and one proton-donor residue (arginine) were identified. The sequence GLPLWFTELDV, located between amino acid residues 619 and 629 of WI5, is a perfect match for the PROSITE protein profile PS00591 for the GH10 active site.

Mutation in *wi5* alters secondary cell wall structure and xylan deposition

WILTED5 encodes endo-1,4-β-xylanase and is mainly expressed in internodes undergoing secondary cell wall deposition. We reasoned that the mutation in *wi5* might alter the cell wall structure of the mutant, leading to stunted growth. Therefore, we compared the cell wall morphology of *wi5* and wild-type plants. Transverse sections derived from the eighth internode (Figure 7A) of field-grown mutant and wild-type plants at the elongating stage were used for these comparisons. Scanning electron microscopy revealed that wild-type sclerenchyma cell walls underlying the epidermis and surrounding the vascular bundles were much thicker than those of *wi5* plants (Figure 7B–G). These results indicate that the *wi5* mutant is primarily deficient in secondary cell wall formation.

To confirm that *WI5* primarily functions in xylan modification, we labeled the eighth internode sections with monoclonal antibodies (Figure 8) LM10 and LM11, which recognize different epitopes on xylan polymers. LM10 is thought to be specific to unsubstituted or lower-substituted xylans, whereas LM11 binds to both lower and higher substituted xylans (Kim and Daniel 2012). These two antibodies predominantly labeled sclerenchyma cells and vascular bundles, which is consistent with the notion that xylan is an abundant polymer in maize secondary cell walls. However, the labeling intensity for both LM10 and LM11 was significantly reduced in *wi5*; this reduction was more dramatic for LM10 compared to LM11. These observations further confirm that the decreased secondary wall thickening in *wi5* is due to a reduction in xylan deposition. Therefore, *WI5* is specifically required for the modification of maize secondary cell walls in sclerenchyma cells and vascular bundles.

To better understand the changes in cell wall components in *wi5*, we analyzed the cellulose, xylan, and lignin contents of the eighth internodes of wild-type and *wi5* plants. No significant difference in cellulose content was detected in the mutant, whereas xylan and lignin contents were reduced (Figure S3). Therefore, *WI5* is required for xylan synthesis and lignin deposition.

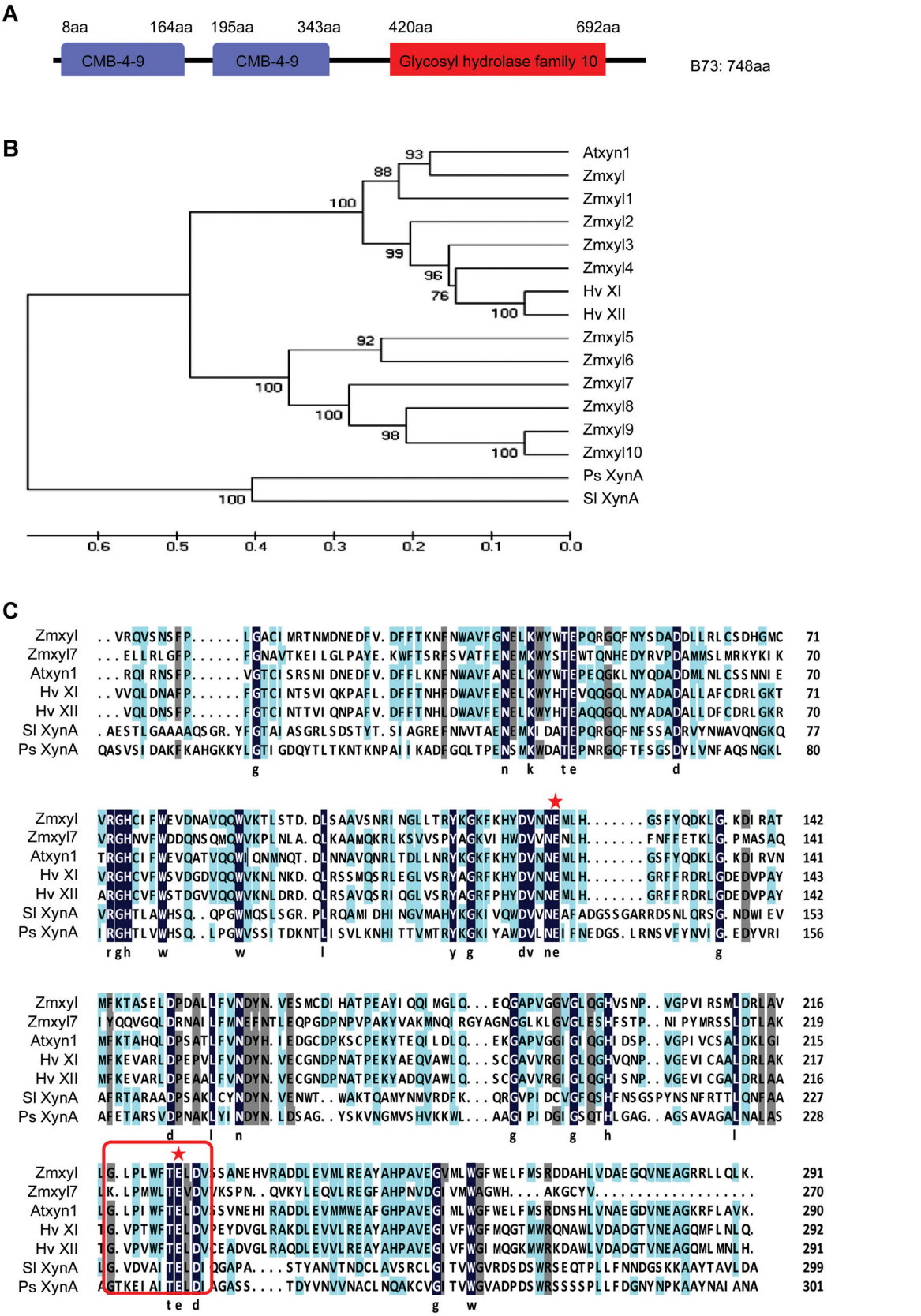

Figure 6. Continued

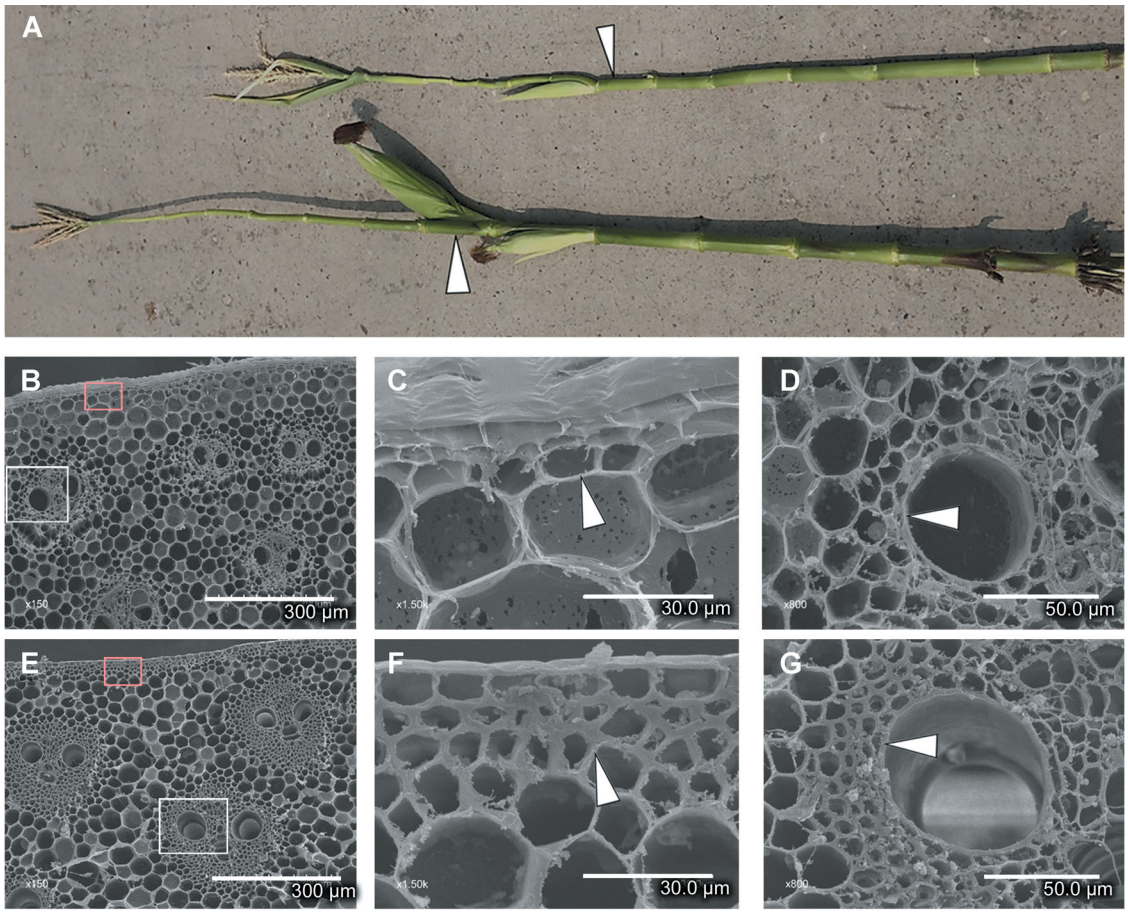

Figure 7. Scanning electron microscopy of the sclerenchyma of an internode
(**A**) *wilty* (*wi5*) and wild-type plants used for observation. The above plant is *wi5*, and below is wild-type. White arrows show the sampling position of *wi5* and wild-type. **(B–G)** Scanning electron micrographs of the sclerenchyma cell of *wi5* and wild-type stems. **(B)** Low-magnification views of *wi5* epidermis and vascular bundles. **(C-D)** Detailed views of *wi5* epidermal sclerenchyma cells shown in red boxes and vascular bundles sclerenchyma cells in white boxes in (**B**). **(E)** Low-magnification views of wild-type epidermis and vascular bundles. **(F-G)** Detailed views of wild-type epidermal sclerenchyma cells shown in red boxes and vascular bundles sclerenchyma cells in white boxes in (**E**). White arrows show the different between *wi5* and wild-type.

To determine whether WI5 has xylanase activity, we expressed wild-type and mutant versions of *WI5* in *Escherichia coli* (TransGen Biotech CD601-01) using a pET30a protein fusion system and purified the proteins using Ni-NTA Agarose (Qiagen 30210). We examined xylanase activity as described by (Bailey et al. (1992). Wild-type proteins had an activity of 11 U/mg under our experimental conditions, whereas the wi5 protein had

Figure 6. Sequence analysis of *WILTY5 (WI5)* encoded protein
(**A**) Protein structure of WI5. WILTY5 contains two carbohydrate-binding domains (CBM4-9) at its C-terminus and one glycosyl hydrolase family 10 (GH10) catalytic domain at its N-terminus. (**B**) Phylogenetic tree of the maize GH10 genes compared to those of *Arabidopsis thaliana*, *Hordeum vulgare*, *Streptomyces lividans*, and *Penicillium simplicissimum*. The numbers at each node represent the bootstrap support (percentage). The scale bar is an indicator of genetic distance based on branch length. (**C**) Multiple sequence alignment of the GH10 catalytic domains of different organisms. The degree of conservation (percent identity) among equivalent residues is indicated as follows: black (100%), dark gray (75%), and light gray (50%). The catalytic residues E-128 and E-236 (corresponding to E-525 and E-626 of the protein sequence of WI5) in *Streptomyces lividans* Xylanase A are indicated by an asterisk. The consensus sequences of the GH10 active site are boxed, corresponding to acid residues 619–629 of WI5. For members of *Zea mays*, please see Table S5.

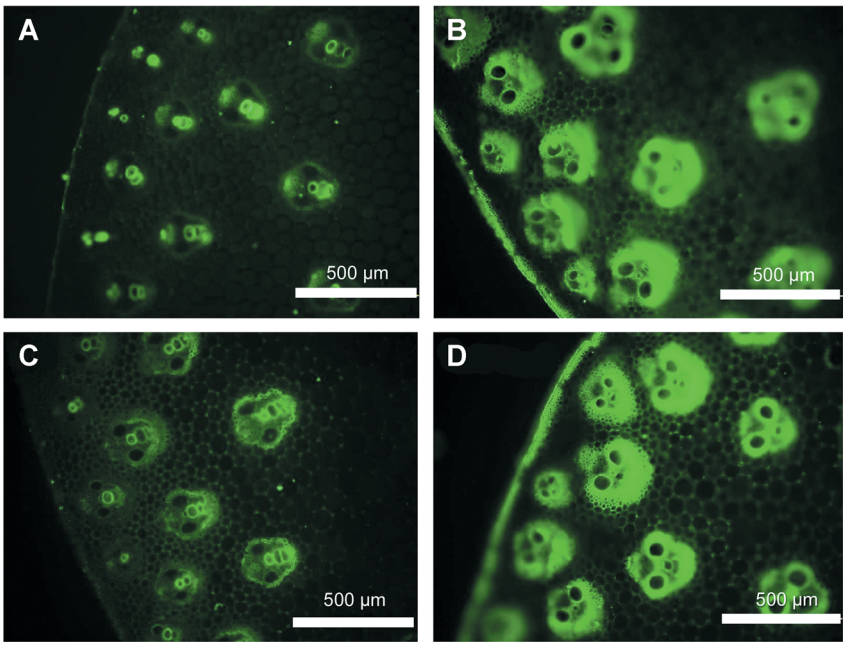

Figure 8. Observation of xylem immunofluorescence from the eighth internode
(**A**) The internode of *wilty (wi5)* was probed with antibody LM10. (**B**) The internode of wild-type was probed with antibody LM10. (**C**) The internode of *wi5* was probed with antibody LM11. (**D**) The internode of wild-type was probed with antibody LM11.

no significant xylanase activity (Figure S4). Thus, the mutant-impaired xylanase activity of WI5 affects the xylan content of the cell wall.

DISCUSSION

WILTED5 is a member of the GH10 family and is highly active in internodes undergoing secondary cell wall thickening

PFAM-based annotation and sequence analysis revealed that WI5 belongs to the GH10 family, with a domain containing two glutamic acid residues essential for catalysis (E525 and E626) and an active site located between amino acid residues 619 and 629. Indeed, we demonstrated the xylanase activity of WI5 *in vitro* (Figure S4).

The regulatory mechanisms of large gene families are more complex than those of smaller gene families, with many members playing partially redundant roles. We identified ten additional *GH10* genes in the maize genome. This gene family does not contain highly conserved sequences. The genes are widespread in the genome, and no recent duplication events were detected. Phylogenetic analysis identified two distinct GH10 subfamilies. *WILTED5* and *Zmxyl1–4* belong to the same clade and share higher sequence identity with *WI5* (33%–53%) than *Zmxyl5–10*, which belongs to another clade, pointing to the functional specialization of different isoforms. Since tissue-specific gene expression patterns might explain specific phenotypes in some cases, we examined the gene expression profiles of *WI5*. *WILTED5* was mainly expressed in maize stems, especially in nonelongated internodes undergoing secondary cell wall thickening, suggesting that WI5 activity is restricted to wall deposition in specialized cells after elongation. In addition, due to the strong mutant phenotype, the possibility of functional redundancy could be eliminated.

Altered cell wall structure and composition lead to stunted growth in *wi5*

The *wi5* mutant displayed stunted growth, with short internodes and a plant height approximately 60% that of wild-type plants. These traits indicate that *WI5* is involved in normal growth and development in maize. Our analysis of the cell wall structure and cell wall components of *wi5* internodes showed that mutations in *WI5* affect the structure and composition of secondary cell walls. The strong differences between

wild-type and *wi5* plants were mainly detected in mechanical tissues, such as sclerenchyma cells and vascular bundles. The sclerenchyma cell wall of the *wi5* mutant was thinner than that of wild-type plants, especially for cells under the epidermal layer. Immunochemical analysis revealed reduced xylan deposition in the secondary cell wall.

These observations indicate that the *wi5* mutation results in developmental changes to the structure and composition of the maize secondary cell wall. A deficiency in the formation of secondary cell walls in *Arabidopsis* usually leads to thinner cell walls (He et al. 2018), collapsed xylem, and globally altered morphology. By contrast, the cell shape and xylem structure did not differ substantially between *wi5* and wild-type plants. Perhaps changes in the secondary cell wall structure have different effects on the overall structure of the xylem in monocot and dicot plants.

Possible role of *WI5* in regulating plant growth and transporting water

The plant cell wall is a dynamic composite structure that provides mechanical support to the plant cell and participates in biotic and abiotic stress responses by remodeling matrix polysaccharides and regulating the cell wall biosynthetic machinery (Wolf et al. 2012). The disruption of the plant cell wall and cell wall enzymes often has obvious consequences on plant growth and development or responses to environmental stimuli (Hamann et al. 2009). The role of the cell wall in resistance to plant diseases and pathogen attack has been extensively studied (Bacete et al. 2018). The pivotal role of the cell wall in mediating abiotic stress responses has also been reported. However, only a few studies have focused on this topic. In the *Arabidopsis lew2* mutant, which has a defect in the cellulose synthase gene *AtCesA8*, xylem cells are collapsed and water transport is impeded, resulting in wilting. The altered cell structure appears to be involved in a feedback response with the accumulation of sugar, proline, and ABA, which enhances drought tolerance (Chen et al. 2005). *LEW3* encodes an α-1,2-mannosyltransferase. The mutation in *lew3* leads to reduced protein glycosylation, impairs cellulose synthesis, and results in xylem collapse, stunted growth, and leaf wilting (Zhang et al. 2009a).

In the current study, we determined that *WI5* encodes an endo-1,4-β-xylanase that remodels the plant cell wall by hydrolyzing cell wall xylan. The disruption of *WI5* affected secondary cell wall structure and composition. The sclerenchyma cell walls were thinner and the xylan and lignin contents were severely reduced in *wi5* compared to wild-type plants. These deficiencies likely result in a lack of structural strength in the xylem, ultimately resulting in defects in water transport capacity. As a result of reduced water uptake from the roots, *wi5* plants were hypersensitive to drought, high temperature, and NaCl, with early wilting leaves, severely inhibited growth, and reduced survival. In addition, *wi5* was highly sensitive to the oxidative stress reagent MV.

Further examination of the effect of the *wi5* mutation on H_2O_2 levels by DAB staining revealed that *wi5* seedling leaves accumulated more H_2O_2 under normal conditions and that *wi5* plants accumulated much higher amounts of H_2O_2 under PEG and MV treatment compared to the wild-type (Figure 3). The *wi5* plants exhibited a clear leaf wilting phenotype under normal growth conditions after the 3-leaf stage. Wilting was initially observed in the leaf margins of *wi5*, and the leaves became quite necrotic and withered under severe conditions. This may be because impaired water transport in the stem led to an abnormal thickening of the cell wall.

The xylan is synthesized in Golgi apparatus and then secreted by vesicles outside the cell. According to the activity of xylan hydrolytic enzyme measured in this experiment, it is speculated that the function of WI5 may modify the synthesis of xylan through its glycoside hydrolytic activity. The specific process is speculated as follows: mature xylan chain which takes part in hemicellulose formation has a particular mature structure, and the xylan precursor produced in the process of xylan synthesis may include some abnormal structures (possibly long beta-1,4 xylose branched chain and too long xylose poly backbone chain). WILTED5 included in a downstream modification pathway, is necessary to process the precursor into the correct structure before it can be secreted out of the cell to participate in the secondary cell wall. Due to the lack of WI5 protein, the xylan precursor could not be processed into mature xylan and could not be secreted out of the cell. The inhibition of the processing of xylan precursor results in the inhibition of the upstream xylan chain synthesis process, which ultimately leads to the reduction of the

accumulation of total xylan content, the failure of the formation of secondary cell walls and the decline of water transport capacity due to the lack of secondary cell walls in xylem, which result in the wilted phenotype of *wi5* mutants.

The inevitable problem is how xylan can be modified rather than hydrolyzed by WI5. Maybe the xylan included in the xylem is glucuronoarabinoxylan which is enriched in side chains, while WI5 plays an hydrolyze active with xylan with fewer side chains. The evidence for this conjecture comes from reports: hydrolysis of xylan from corn cob requires a combination of glycolytic enzymes from other families that hydrolyze glucuronic acids and Arabian side chains (Rogowski et al. 2015). Further, in our previous preliminary tests to determine xylan activity (data not shown), WI5 showed no hydrolytic activity for xylan (glucuronoarabinoxylan) from corn cob, but showed significant activity for xylan from beechwood which lacks side chains.

In summary, we identified an endo-1,4-xylanase gene that plays an essential role in secondary cell wall synthesis in maize, as demonstrated by both morphological and molecular analyses.

MATERIALS AND METHODS

Plant materials and growth conditions

The *wi5* mutant was isolated from M2 population of W22 background *Mutator* transposon mutants (*Mu9*) crossed with inbred line Zong31. The plants were grown in the Shang Zhuang Experimental Station of the China Agricultural University for phenotypic observation and measurement of physiological indicators. For fine mapping, *wi5* was backcrossed into the B73 genetic background to generate a BC_1F_1 backcross population which included more than 4,000 individual plants. *wilted5* was backcrossed into the B73 genetic background for four generations and selfing once to generate a BC_4F_2 population. The homozygotes (*wi5*/*wi5*) and heterozygotes (*wi5*/+) from the BC_4F_2 population were used as the mutant and wild-type, respectively.

To observe the phenotypes of *wi5* under different stress treatments, *wi5* and wild-type plants were planted side-by-side in the same pots in the greenhouse. Water was continuously supplied until the plants reached the 5-leaf stage. The plants were subsequently treated with drought, high temperature (42°C), 250 mmol/L NaCl, or 50 μmol/L MV. The plants were photographed at different time points before and after treatment.

Measurement of water loss of detached leaves

Leaves of the same position were detached from 3-week-old wild-type and *wi5* seedlings and their fresh weights were measured (at t = 0). Then the weight was measured every 30 min for 6 h in a ventilated dry room. Wild-type and *wi5* plants were each measured three times. Water loss was calculated as: water loss rate = (Ws−Wt)/Ws (Ws = fresh weight of leaf at time = 0; Wt = weight of detached leaf at time t).

Measurement of leaf ABA content

Leaves of the same position were detached from wild-type and *wi5* seedlings planted in the same pot and their ABA content was measured under the followed conditions: D0, 3-week-old seedlings watered normally; D20, 20 d drought treatment; D30, 30 d drought treatment; Re-watering for 10 d. Wild-type and *wi5* plants were measured three times each. ABA content was measured as previously described (Zhang et al. 2009b).

Histochemical analysis

Hydrogen peroxide accumulation was measured by DAB staining (Sigma). Leaves were submerged in 1.0 mg/mL DAB solution and incubated in darkness at room temperature for 6–8 h. To visualize cell death, leaves collected from *wi5* and wild-type plants at the 10-leaf stage were submerged in lactophenol Trypan blue solution (5 mL lactic acid, 10 mL of 50% glycerol, 1 mg Trypan blue (Sigma), and 5 mL phenol) at 30°C for 2–3 h. After each staining, the leaves were destained for 10 min in boiling 95% ethanol. Samples were observed under a dissecting microscope (Olympus, SZX16-DP72).

Genetic analysis and marker development

A fine mapping population including 4,000 BC_1F_1 segregation plants was constructed by crossing *wi5* with B73. Genomic DNA was extracted and subjected to cosegregation analysis using available SSR markers listed in http://www.maizegdb.org. New SSR markers were identified using the SSR Hunter 1.3 Simple

Sequence Repeat Search tool and designed using Primer 5.0 based on B73 genome sequence information in http://ensembl.gramene.org/Zea_mays/Info/Index. CAPS markers were developed using SNP2CAPS software based on sequence comparisons between the *wi5* mutant and B73 according to the B73 sequence in http://www.ncbi.nlm.nih.gov.

Copy number analysis and testing of a transgenic complementation event

A homozygous T3 generation line was isolated from a T2 individual. Genomic DNA was extracted from 14-d-old seedlings of the homozygous T3 line and *wi5*. The DNA was diluted to 100 ng/μL and digested with FastDigest HindIII (Thermo Scientific™ FD0504). The following primers were used for ddPCR: HMGA-F1, 5′-GAAATCCCTGAGCGAGTCGGTA-3′ and HMGA-R1, 5′-AGTAACAACGCAATTGAAGCATC-3′ as the internal reference; and WI5_DDPCR_F1, 5′-TGGCGCAGGAGTC CCTGGAG-3′ and WI5_DDPCR_R1, 5′-GAGACCTGGTAGG TGGCGTAGA-3′ for amplification of both endogenous and exogenous *WI5*. Sample amplification and data analysis were performed using QX200 ddPCR EvaGreen Supermix (Bio-Rad 186-3022) and the QX200 Droplet Digital PCR System (Bio-Rad 186-4001).

Sequence and phylogenetic analyses

GH10 genes were identified by searching the whole genome sequence database of maize using DNA or protein sequences of the maize *WI5* gene as queries. Gene prediction was performed using FGENESH (Salamov and Solovyev 2000). Subcellular localization was predicted with ProtComp v. 9.0 (www.softberry.com). Multiple amino acid sequence alignments and phylogenetic analyses were performed using DNAMAN version 6.0 (LynnonBiosoft) and MEGA software version 4.0.

Xylanase activity assay

The complementary DNA (cDNA) fragments from wild-type and *wi5* plants were amplified and inserted into expression plasmid pET30a, which was expressed in *E. coli* (TransGen Biotech CD601-01). The protein was purified using Ni-NTA Agarose (Qiagen 30210). Purified protein was diluted to 0.2 mg/mL. The xylanase substrate used in this experiment was xylan produced from a 10 mg/mL solution (Megazyme P-XYLNBE-10G) dissolved in sodium acetate buffer, pH 5.0 at 0.1 mol/L. A 200 μL aliquot of protein solution was mixed with 1.8 mL substrate, incubated at 50°C for 10 min and cooled in ice water. A solution containing sodium acetate buffer instead of protein served as the reagent blank. A standard curve was constructed using 0, 0.2, 0.4, 0.6, 0.8, and 1.0 mL of 1 mg/mL xylose dissolved in 0.1 mol/L, pH 5.0 sodium acetate and diluted with sodium acetate buffer to 2 mL, combined with 3 mL 3,5-Dinitrosalicylic acid, incubated in a boiling water bath for 10 min, and diluted with water to 15 mL. The color produced at 540 nm was measured against the reagent blank and the released xylose was calculated based on the standard curve: 1 U represents the amount of enzyme that 1 μmol xylose releases per minute.

RT-PCR and real-time PCR

Total RNA was extracted from various organisms and subjected to reverse-transcription. The RNA was digested with DNaseI for 40 min at 37°C. The reaction was stopped by adding stop solution and was then incubated at 65°C for 10 min, and the RNA was reverse-transcribed into cDNA with oligos and avian myeloblastosis virus reverse transcriptase. For RT-PCR, *tubulin* primers were used as a control (5′-GTGTCCTGTCCACCC ACTCTCT-3′ and 5′-GGAACTCGTTCACATCAACGTTC-3′). Expression analysis of *WI5* was carried out using specific primers (5′-CGGTAACTACTGTCTTTCGAGGAA-3′ and 5′-TGTTGTGATACATAAAGCACGCAT-3′). Each 30 μL reaction included 0.5 μm of each primer and 1× SYBR Green PCR Master Mix (Takara). The reactions were carried out in a Real-Time PCR System as follows: 95°C for 2 min, 40 cycles of 95°C for 15 s, 60°C for 34 s, and 72°C for 15 s.

Transcriptome analysis

The eighth internodes and 13th leaves of *wi5* and wild-type plants at the 13-leaf stage were sampled for RNA-seq library construction. An average of 1.98 G clean data was aligned to the B73 V3 reference genome. PCA was performed based on gene expression level. DEGs were identified using DESeq2, and KEGG (https://www.kegg.jp/) was used for pathway enrichment analysis of the DEGs.

Xylan immunolocalization

Stem sections were incubated with LM10 and LM11 antibodies (Plant Probes; 1/20 dilution) for 1 h (Kim and Daniel 2012). The samples were washed in

phosphate-buffered saline and incubated for 1 h with fluorescein isothiocyanate-conjugated anti-rat secondary antibody (1/100 dilution; Jackson ImmunoResearch). The samples were visualized using a Leica fluorescence microscope.

Cell wall component analysis

The eighth internodes of *wi5* and wild-type plants at the 13–15-leaf stage were dried and ball-milled into a powder. The cell wall residues were treated with pullulanase M1 (Megazyme) and α-amylase (Sigma) in 0.1 mol/L sodium acetate buffer (pH 5.0) overnight to remove starch. To analyze neutral sugar and cellulose contents, the alcohol-insoluble residues (AIRs) were hydrolyzed with trifluoroacetic acid. The supernatants were reduced and analyzed by gas chromatography – mass spectrometry (Agilent) to determine the monosaccharide content as previously described. The remaining material was treated with Updegraff reagent and hydrolyzed with 72% sulfuric acid to measure the cellulose content. The lignin content was measured using the acetyl bromide method (Foster et al. 2010).

Injury flow test

WILTED5 and wild-type kernels were surface disinfected in 10% (v/v) H_2O_2 for 30 min, pre-germinated in saturated $CaSO_4$ for 6 h, and washed three times in pure water. Kernels were then germinated in darkness between two layers of wet filter paper. The endosperm was removed from seedlings exhibiting the same growth trends and the embryos were grown in liquid Murashige and Skoog medium until they reached the 3-leaf stage. The embryos were then transferred into a 100% relative humidity environment and the middle of their hypocotyls were cut. Injury flow was collected for 4 h. Roots of detected seedlings were dried at 42°C and weighed. Injury flow rate was calculated as: injury flow (μL)/time (h)/weight of dehydrated root (g).

ACKNOWLEDGEMENTS

This work was supported by grants from the National Key Research and Development Program of China (2016YFD0101803) and the National Natural Science Foundation of China (31971959, 31421005; 31601313; 91735301).

AUTHOR CONTRIBUTIONS

X. H., H. Z., and Y. C. designed the experiments. X. H., Y. C., and X. L. performed most of the experiments and analyzed the data. The other authors assisted in the experiments and discussed the results. X. H., Y. C., and H. Z. wrote the manuscript. All authors read and approved the manuscript.

REFERENCES

Andriotis VME, Rejzek M, Barclay E, Rugen MD, Field RA, Smith AM (2016) Cell wall degradation is required for normal starch mobilisation in barley endosperm. **Sci Rep** 6: 33215

Bacete L, Melida H, Miedes E, Molina A (2018) Plant cell wall-mediated immunity: Cell wall changes trigger disease resistance responses. **Plant J** 93: 614–636

Bailey MJ, Biely P, Poutanen K (1992) Interlaboratory testing of methods for assay of xylanase activity. **J Biotechnol** 23: 257–270

Cantarel BL, Coutinho PM, Rancurel C, Bernard T, Lombard V, Henrissat B (2009) The Carbohydrate-Active EnZymes database (CAZy): An expert resource for glycogenomics. **Nucleic Acids Res** 37: D233–D238

Caspers MPM, Lok F, Sinjorgo KMC, van Zeijl MJ, Nielsen KA, Cameron-Mills V (2001) Synthesis, processing and export of cytoplasmic endo-beta-1,4-xylanase from barley aleurone during germination. **Plant J** 26: 191–204

Chen Z, Hong X, Zhang H, Wang Y, Li X, Zhu JK, Gong Z (2005) Disruption of the cellulose synthase gene, AtCesA8/IRX1, enhances drought and osmotic stress tolerance in *Arabidopsis*. **Plant J** 43: 273–283

Chien Van H, Antonio Leyva-Gonzalez M, Osakabe Y, Uyen Thi T, Nishiyama R, Watanabe Y, Tanaka M, Seki M, Yamaguchi S, Nguyen Van D, Yamaguchi-Shinozaki K, Shinozaki K, Herrera-Estrella L, Lam-Son Phan T (2014) Positive regulatory role of strigolactone in plant responses to drought and salt stress. **Proc Natl Acad Sci USA** 111: 851–856

Ding YR, Cai YJ (2013) Conformational dynamics of xylanase a from Streptomyces lividans: Implications for TIM-barrel enzyme thermostability. **Biopolymers** 99: 594–604

Foster CE, Martin TM, Pauly M (2010) Comprehensive compositional analysis of plant cell walls (Lignocellulosic biomass) part I: Lignin. **J Vis Exp** 37: e1e745

Glass M, Barkwill S, Unda F, Mansfield SD (2015) Endo-beta-1,4-glucanases impact plant cell wall development by

influencing cellulose crystallization. **J Integr Plant Biol** 57: 396–410

Guo C, Luo C, Guo L, Li M, Guo X, Zhang Y, Wang L, Chen L (2016) OsSIDP366, a DUF1644 gene, positively regulates responses to drought and salt stresses in rice. **J Integr Plant Biol** 58: 492–502

Hamann T, Bennett M, Mansfield J, Somerville C (2009) Identification of cell-wall stress as a hexose-dependent and osmosensitive regulator of plant responses. **Plant J** 57: 1015–1026

He J-B, Zhao X-H, Du P-Z, Zeng W, Beahan CT, Wang Y-Q, Li H-L, Bacic A, Wu A-M (2018) KNAT7 positively regulates xylan biosynthesis by directly activating IRX9 expression in *Arabidopsis*. **J Integr Plant Biol** 60: 514–528

Juturu V, Wu JC (2012) Microbial xylanases: Engineering, production and industrial applications. **Biotechnol Adv** 30: 1219–1227

Kim JS, Daniel G (2012) Immunolocalization of hemicelluloses in Arabidopsis thaliana stem. Part I: Temporal and spatial distribution of xylans. **Planta** 236: 1275–1288

Kognole AA, Payne CM (2015) Cello-oligomer-binding dynamics and directionality in family 4 carbohydrate-binding modules. **Glycobiology** 25: 1100–1111

Lerouxel O, Cavalier DM, Liepman AH, Keegstra K (2006) Biosynthesis of plant cell wall polysaccharides—a complex process. **Curr Opin Plant Biol** 9: 621–630

Li W-Q, Zhang M-J, Gan P-F, Qiao L, Yang S-Q, Miao H, Wang G-F, Zhang M-M, Liu W-T, Li H-F, Shi C-H, Chen K-M (2017) CLD1/SRL1 modulates leaf rolling by affecting cell wall formation, epidermis integrity and water homeostasis in rice. **Plant J** 92: 904–923

Li YB, Suen DF, Huang CY, Kung SY, Huang AHC (2012) The maize tapetum employs diverse mechanisms to synthesize and store proteins and flavonoids and transfer them to the pollen surface. **Plant Physiol** 158: 1548–1561

Liu S, Zheng L, Xue Y, Zhang Q, Wang L, Shou H (2010) Overexpression of OsVP1 and OsNHX1 increases tolerance to drought and salinity in rice. **J Plant Biol** 53: 444–452

Liu Y, You S, Taylor-Teeples M, Li WL, Schuetz M, Brady SM, Douglas CJ (2014) BEL1-LIKE HOMEODOMAIN6 and KNOTTED ARABIDOPSIS THALIANA7 interact and regulate secondary cell wall formation via repression of REVOLUTA. **Plant Cell** 26: 4843–4861

Ma Z, Song T, Zhu L, Ye W, Wang Y, Shao Y, Dong S, Zhang Z, Dou D, Zheng X, Tyler BM, Wang Y (2015) A phytophthora sojae glycoside hydrolase 12 protein is a major virulence factor during soybean infection and is recognized as a PAMP. **Plant Cell** 27: 2057–2072

Pollet A, Delcour JA, Courtin CM (2010) Structural determinants of the substrate specificities of xylanases from different glycoside hydrolase families. **Crit Rev Biotechnol** 30: 176–191

Rock CD, Ng PPF (1999) Dominant Wilty mutants of *Zea mays* (Poaceae) are not impaired in abscisic acid perception or metabolism. **Am J Bot** 86: 1796–1800

Rogowski A, Briggs JA, Mortimer JC, Tryfona T, Terrapon N, Lowe EC, Basle A, Morland C, Day AM, Zheng H, Rogers TE, Thompson P, Hawkins AR, Yadav MP, Henrissat B, Martens EC, Dupree P, Gilbert HJ, Bolam DN (2015) Glycan complexity dictates microbial resource allocation in the large intestine. **Nat Commun** 6: 7481

Salamov AA, Solovyev VV (2000) Ab initio gene finding in Drosophila genomic DNA. **Genome Res** 10: 516–522

Seifert GJ, Blaukopf C (2010) Irritable walls: The plant extracellular matrix and signaling. **Plant Physiol** 153: 467–478

Suzuki M, Kato A, Nagata N, Komeda Y (2002) A xylanase, AtXyn1, is predominantly expressed in vascular bundles, and four putative xylanase genes were identified in the *Arabidopsis thaliana* genome. **Plant Cell Physiol** 43: 759–767

Venturas MD, Sperry JS, Hacke UG (2017) Plant xylem hydraulics: What we understand, current research, and future challenges. **J Integr Plant Biol** 59: 356–389

Vogel J (2008) Unique aspects of the grass cell wall. **Curr Opin Plant Biol** 11: 301–307

Wan Q, Parks JM, Hanson BL, Fisher SZ, Ostermann A, Schrader TE, Graham DE, Coates L, Langan P, Kovalevsky A (2015) Direct determination of protonation states and visualization of hydrogen bonding in a glycoside hydrolase with neutron crystallography. **Proc Natl Acad Sci USA** 112: 12384–12389

Wolf S, Hématy K, Höfte H (2012) Growth control and cell wall signaling in plants. **Annu Rev Plant Biol** 63: 381–407

Yuan Z, Yao X, Zhang DB, Sun Y, Huang H (2007) Genome-wide expression profiling in seedlings of the *Arabidopsis* mutant uro that is defective in the secondary cell wall formation. **J Integr Plant Biol** 49: 1754–1762

Zhang J, Zhang H, Srivastava AK, Pan Y, Bai J, Fang J, Shi H, Zhu J-K (2018) Knockdown of rice microRNA166 confers drought resistance by causing leaf rolling and altering stem xylem development. **Plant Physiol** 176: 2082–2094

Zhang M, Henquet M, Chen Z, Zhang H, Zhang Y, Ren X, Van Der Krol S, Gonneau M, Bosch D, Gong Z (2009a) LEW3, encoding a putative α-1, 2-mannosyltransferase (ALG11) in N-linked glycoprotein, plays vital roles in cell-wall biosynthesis and the abiotic stress response in *Arabidopsis thaliana*. **Plant J** 60: 983–999

Zhang M, Yuan B, Leng P (2009b) The role of ABA in triggering ethylene biosynthesis and ripening of tomato fruit. **J Exp Bot** 60: 1579–1588

Zhang SS, Sun L, Dong XR, Lu SJ, Tian WD, Liu JX (2016) Cellulose synthesis genes CESA6 and CSI1 are important for salt stress tolerance in *Arabidopsis*. **J Integr Plant Biol** 58: 623–626

Zhu JH, Lee BH, Dellinger M, Cui XP, Zhang CQ, Wu S, Nothnagel EA, Zhu JK (2010) A cellulose synthase-like protein is required for osmotic stress tolerance in *Arabidopsis*. **Plant J** 63: 128–140

SUPPORTING INFORMATION

Additional Supporting Information may be found online in the supporting information tab for this article: http://onlinelibrary.wiley.com/doi/10.1111/jipb.12923/suppinfo

Figure S1. *WI5* gene copy numbers of positive transgenic event and *wi5*

Gene copy numbers were calculated by the ratio of *WI5* to reference. F3, homozygous plant by crossed positive T0 plants with *wi5* plants and two-generation self-crossing.

Figure S2. Transcriptome analysis of leaves and internodes of wild-type and *wi5*

(**A**) Principal component analysis. (**B**) Venn diagram of Sample_WT_S vs Sampel_wi5_S and Sample_WT_L vs Sample_wi5_L. (**C**) Pathway enrichment of down-regulated genes (left) and up-regulated genes (right). Sample_WT_L and Sample_wi5_L: leaf data of wild-type and *wi5* mutant; Sample_WT_S and Sampel_wi5_S: Internodes data of wild-type and *wi5* mutant.

Figure S3. Comparison of cell wall component between wild-type and *wi5* in eighth internode

Cellulose, xylan, and lignin contents of the eighth internodes of wild-type and *wi5* plants. Error bars indicate ± *SE* ($n = 3$). Student's *t*-test (*$P < 0.05$, **$P < 0.01$, ***$P < 0.001$).

Figure S4. Xylanase activity of wild-type and *wi5*

1 U represents amount of enzyme that releases 1 μmol xylose per minute. CK represents blank tested additional three times for error calibration. Error bars indicate ± *SE* ($n = 3$). Student's *t*-test (*$P < 0.05$, **$P < 0.01$, ***$P < 0.001$).

Table S1. Genetic pattern of *wi5*

Table S2. The photosynthesis indexes of wild-type plant and *wi5* mutant

Table S3. Markers used in the positional cloning of *WI5* gene

Table S4. Statistical analysis of transgenic F2 generation segregation ratio

Table S5. Overview of the 11 members of the GH10 family identified in maize

Scan using WeChat with your smartphone to view JIPB online

Scan with iPhone or iPad to view JIPB online